Resonance broadening and tuning of split ring resonators by top-gated epitaxial graphene on SiC substrate

Semih Cakmakyapan, Levent Sahin, Francesco Pierini, Wlodek Strupinski, and Ekmel Ozbay

---

Articles you may be interested in

The correlation of epitaxial graphene properties and morphology of SiC (0001)
J. Appl. Phys. **115**, 043527 (2014); 10.1063/1.4863796

Electronic transport properties of top-gated epitaxial-graphene nanoribbon field-effect transistors on SiC wafers
J. Vac. Sci. Technol. B **32**, 012202 (2014); 10.1116/1.4861379

The influence of substrate morphology on thickness uniformity and unintentional doping of epitaxial graphene on SiC
Appl. Phys. Lett. **100**, 241607 (2012); 10.1063/1.4729556

Effects of substrate orientation on the structural and electronic properties of epitaxial graphene on SiC(0001)
Appl. Phys. Lett. **98**, 222109 (2011); 10.1063/1.3597356

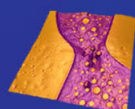Substrate doping effects on Raman spectrum of epitaxial graphene on SiC
J. Appl. Phys. **107**, 034305 (2010); 10.1063/1.3283922
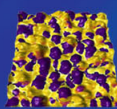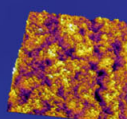
Resonance broadening and tuning of split ring resonators by top-gated epitaxial graphene on SiC substrate

Semih Cakmakyapan,[1,2,a)] Levent Sahin,[2,3] Francesco Pierini,[2] Wlodek Strupinski,[4] and Ekmel Ozbay[1,2,3]

[1]*Department of Physics, Bilkent University, 06800 Ankara, Turkey*
[2]*Nanotechnology Research Center, Bilkent University, 06800 Ankara, Turkey*
[3]*Department of Electrical and Electronics Engineering, Bilkent University, 06800 Ankara, Turkey*
[4]*Institute of Electronic Materials Technology, Wolczynska 133, 01-919 Warsaw, Poland*

Split ring resonators (SRRs) are subwavelength structures that are able to localize and enhance the electromagnetic wave. Controlling the plasmonic resonance behavior of metallic nanostructures, such as SRRs, plays an important role in optoelectronics and nanophotonics applications. Electrically tunable carrier concentration of graphene provides hybrid devices, where the plasmonic structures and graphene are combined. In this paper, we report the design, fabrication, and measurement of a device comprising a SRR array on epitaxial graphene. We obtained resonance broadening and tuning of split ring resonators by utilizing an epitaxial graphene transistor with transparent top-gate. © 2013 AIP Publishing LLC. [http://dx.doi.org/10.1063/1.4828499]

Graphene is a monolayer of carbon atoms that are arranged in a two-dimensional honeycomb lattice. This 2D material can be used for wrapping up into fullerenes (0D), for rolling into nanotubes (1D), or for stacking into 3D graphite.[1] Since graphene has interesting electrical and mechanical properties, it has been an attractive research material in recent years. An electron inside a monolayer graphene sheet has zero effective mass,[2] and it can travel for micrometers without scattering even at room temperature.[3,4] Graphene also exhibits many interesting and exotic properties ranging from ballistic electronic transport[5–7] to the anomalous quantum Hall effect in electrical transport[2,7] and tunable interband transitions.[8,9] Graphene has exceptional optical properties. For instance, graphene exhibits saturable absorption constant as a consequence of Pauli blocking.[10–12] Moreover, non-equilibrium carrier results in hot luminescence.[13,14] Graphene is a versatile optical material for nanophotonics applications[3] such as metamaterials,[15] photodetectors,[16] light emitting devices, and ultrafast lasers.[17] In particular, graphene with its planar nature attracts an increasing research interest as a promising tool for nano-plasmonics and nanoscale electronics.[18,19] Pioneering works of graphene were focused on the single particle excitation of electrons. On the other hand, the plasmonic properties of graphene layer, which is a result of the collective excitations of 2D massless electrons, has become an emerging research area in recent years. Plasmonic resonances in graphene give outstanding potential for designing optoelectronic devices by its remarkably high absorption.[3,20,21] Electrical response at terahertz frequencies are high enough to design plasmonic devices.[5,22] However, the electrical control of plasmon resonance becomes a challenge at optical frequencies as a result of drastically reduced free electron responses with increasing frequency. Graphene, which is a zero bandgap semiconductor,[8,9,22] is a great candidate to overcome this challenge. Since high frequency interband transition in graphene can be exploited through electrical gating,[22] plasmon resonance of graphene-hybrid device like split ring resonators (SRRs) can be modulated by applying gate voltage,[23,24] which changes the carrier concentration, thus modulating the optical conductivity.[25,26] Surface plasmons have the characteristics of concentrating light into a subwavelength volume, which is one of the main tools of plasmonics.[1,22] Plasmons in graphene is an active research field,[20,21,27–29] and it is desired to control the plasmon resonances for optical switch applications.

Here, we report the optical response of SRR arrays on epitaxial graphene. Strong localized fields around SRR-based structures couple to the incident field through a resonant process, causing a strong localization of electromagnetic waves. SRRs enhance the incident field and therefore increase the interaction between light and graphene, where the asymmetric broadening and shifting of transmission spectra are studied.

The graphene sample in this study is grown by the sublimation method on 4H-SiC polytype. The sample is intercalated by hydrogen, where the temperature of sublimation is $1600\,^\circ$C, and the reactor pressure is set to 50 mbar. The sample is p-type with a carrier concentration of 1.3×10^{13} cm^{-2}, and the mobility is measured to be 3234 cm^2/Vs. In terms of the fabrication of the samples, first of all, a chromium mask is designed and fabricated by electron beam lithography to be further used in optical lithography during device fabrication. Fabrication steps are schematically shown in Figure 1 starting from the Raman measurement of the bare graphene, where characteristic 2D and G peaks of graphene are visible along with the SiC peak. The reverse photolithography of the ohmic contacts are performed to form the source and drain contacts with a positive-tone photo-resist. After the development, 20 nm titanium and 80 nm gold are deposited by the electron beam evaporation, followed by a standard lift-off process. $100\,\mu$m $\times$ $100\,\mu$m ohmic contacts are $120\,\mu$m apart from each other, abbreviated as S and D in Fig. 1. After the ohmic contact metallization, mesa etch lithography is performed in order to isolate the devices electrically from each other. The sample

a)Author to whom correspondence should be addressed. Electronic mail: semihc@bilkent.edu.tr
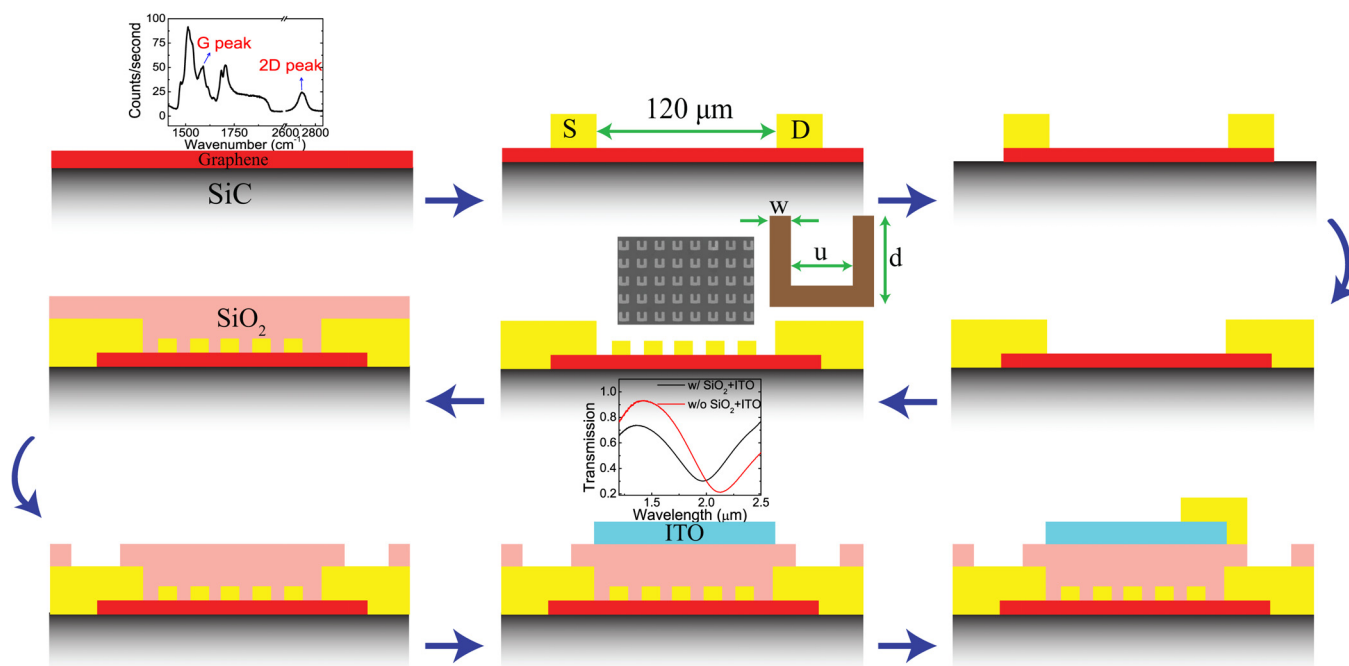
103, 181116-1

FIG. 1. Schematic of the device fabrication steps.

is exposed to oxygen plasma for 20 s by using Inductively Coupled Plasma Reactive Ion Etching (ICP-RIE), where the RF power is 50 W and ICP source power is 100 W. Then, another photolithography for interconnect metallization, which consists of 20 nm titanium and 200 nm gold, is performed for the probing and wire bonding purposes during the measurements. This step provides large pads connected to source and drain contacts. Later, the fabrication of the split ring resonators is carried out by electron beam lithography on the active graphene region. 15 kV accelerating voltage and 10 μm aperture are used for the exposure. After electron beam lithography, 5 nm titanium as a buffer layer and 40 nm gold are evaporated. A scanning electron microscopy (SEM) image of an SRR array is shown as an inset of Fig. 1. Then, the dielectric passivation step is carried out with 100 nm SiO$_2$. This process is performed in two steps, where 50 nm SiO$_2$ is deposited by electron beam evaporation and 50 nm SiO$_2$ is deposited by sputter. Several trials showed that the gate leakage cannot be avoided by doing the electron beam evaporation step only. The reason is that the electron beam evaporation provides a very directional deposition on the surface, and it does not cover the sides of the metallic structures and the bumps due to the gold evaporation, and, hence, it leads to the leakage current caused by the SRRs, when the gate fabrication is completed. However, sputtering as a second step entirely covers all of the sides as well as the bumps on the metal surfaces such as a blanket, thus providing a proper isolation layer. The reason why electron beam evaporation is used before the sputtering is to protect the graphene surface from the plasma exposure of the sputter system. Argon plasma is created and used during the sputtering process. It was shown in Refs. 30 and 31 that the graphene is highly sensitive to Ar plasma, which can create defect sites on the surface. After the dielectric deposition steps, another etch process is performed in order to physically reach the source and drain contacts, as shown in the left bottom corner of Fig. 1. CHF$_3$ plasma is

used, where the RF power is set to 100 W, and ICP power is set to 200 W. Since the SiC substrate is semi-insulating, a top-gate is needed to apply the bias voltage. Indium tin oxide (ITO) is chosen to be the gate material due to its conductivity and transparency. Photolithography process is performed so that a 100 nm-thick ITO window just above the active graphene region can be deposited by sputtering. As a final process step, a gold metal pad connected to the ITO is fabricated with the same steps followed in source-drain interconnect metallization.

IV measurements are performed in order to investigate the gate-dependent DC modulation performance of the devices. The results are plotted in Fig. 2. Fig. 2(a) shows the change of the IV characteristics between source and drain contacts under different gate voltages. Each curve is linear and hence has a constant resistance, which is the indication of the ohmic contact characteristics. Resistance increases up to 60 V of gate voltage and then decreases for higher gate voltages. This turning point can be seen clearly from the saddle point of Fig. 2(b). It can be concluded that the Dirac point, which is the charge neutrality point, is around 60 V. Measurements are performed up to 70 V in order not to exceed the breakdown voltage of SiO$_2$. Gate current at V$_{gate}$ = 60 V is measured to be on the orders of 10^{-11} A, as shown in the inset of Figure 2(b), which proves that there is no gate leakage, and the dielectric passivation step works well.

Transmission of SRRs before and after the deposition of SiO$_2$ and ITO layers is measured, and they are shown as an inset in Fig. 1. A red shift about 200 nm at the resonance wavelength is observed after the deposition of these two layers.

In this study, there are two resonant devices that operate at different wavelengths. Resonance wavelength of device 1 is at around 2 μm, where u = 100 nm, w = 42 nm, d = 180 nm, and periodicity is 307 nm in both x and y-directions.
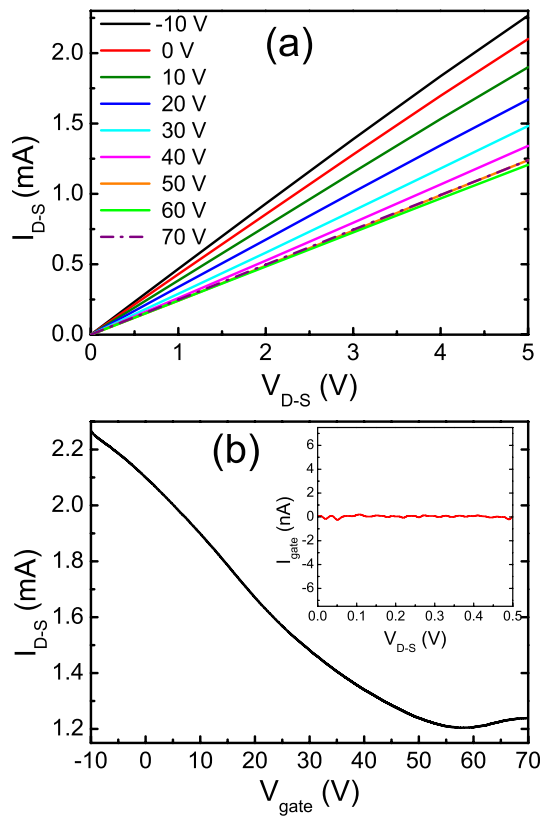
FIG. 2. DC-IV Measurements (a) drain voltage vs drain current, (b) gate voltage vs drain current; inset shows drain voltage vs gate current.

Resonance wavelength of device 2 is around $4\,\mu m$, where $u = 130\,nm$, $w = 165\,nm$, $d = 420\,nm$, and periodicity is $820\,nm$ in both x and y-directions. The transmission spectra of these two devices under different gate voltage differences, ΔV, are shown in Fig. 3, where the resonance dips are enlarged in the inset. Here, ΔV is defined as $\Delta V = V_{gate} - V_{CNP}$, where V_{CNP} is the voltage value at the charge neutrality point. It should be noted that the curves change their shape asymmetrically with applied voltage. 28 nm blue shift at the resonance wavelength is measured and demonstrated in the inset of Fig. 3(b). The reason of this shift and the asymmetric behavior is the higher sensitivity of graphene to the light at higher wavelengths.

Line width and quality factor variations with respect to gate voltage difference are plotted in Fig. 4. $\Delta\lambda$ is the line width difference with respect to the line width of the curve measured at $\Delta V = 0$. The line width decreases, and as a result the quality factor increases, as ΔV decreases, which is to say that the curves narrow down away from the charge neutrality point. An incident photon having an energy $\hbar\omega > 2E_F$ can be absorbed because it generates an electron-hole pair. Fermi energy, E_F, approaches zero at the charge neutrality point, which results in more interband transitions due to the incident photons and hence absorption increases. The results presented in Figs. 3 and 4 are consistent with the theory. Transmission curve at the Dirac point, where $\Delta V = 0\,V$, is the broadest one having the lowest quality factor, as expected. The reason is that the absorption is the highest for this case.

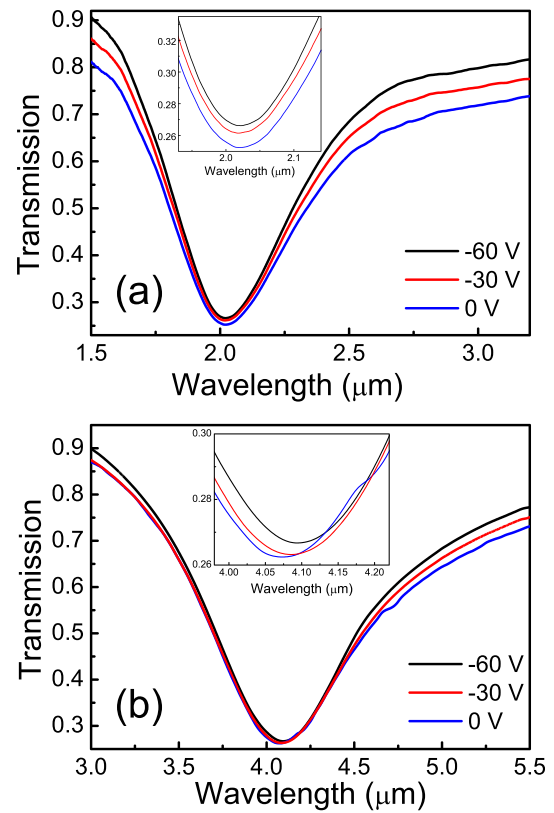Finite difference time domain (FDTD) simulations are carried out in order to verify experimentally observed

transmission spectra. The results are shown in Fig. 5 for both device 1 and device 2. Graphene is modeled as an effective medium by using random phase approximation (RPA) model.[25,26] Real and imaginary parts of refractive index are

FIG. 3. Transmission measurements under different gate voltage differences, ΔV, for (a) device 1, and (b) device 2.
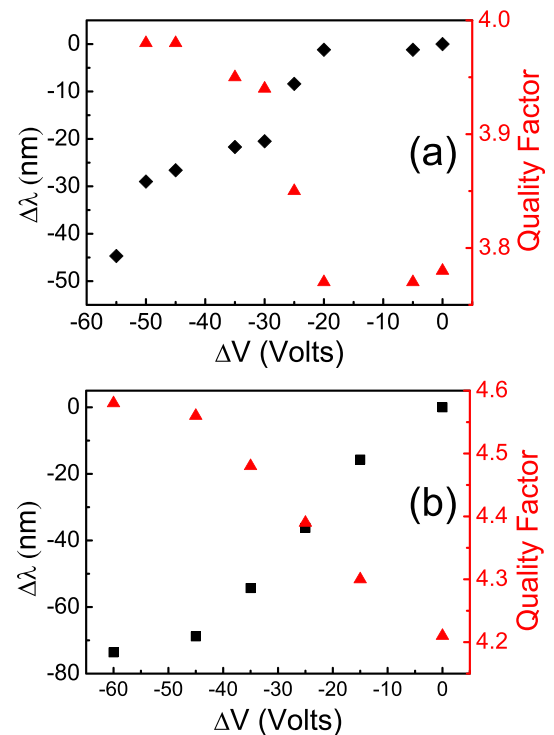

FIG. 4. Line width difference, $\Delta\lambda$, and quality factor variation for (a) device 1 and (b) device 2 (Black squares represent the line width difference, and red triangles represent the quality factor.).
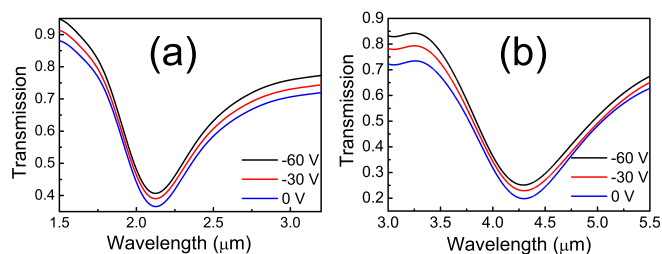
FIG. 5. Calculated transmission data under different gate voltage differences for (a) device 1, and (b) device 2.

extracted from the optical conductivity of graphene, which is a function of Fermi energy. The relation between the Fermi energy and the sheet carrier concentration of graphene is represented as $E_F = \hbar \nu_F \sqrt{\pi N}$.[2,6] Furthermore, it is shown in Ref. 8 that the carrier concentration and the voltage are linearly proportional to each other. We used these two relations in our simulations in order to find out the corresponding Fermi energy for each applied voltage. Simulations show a good correlation with the measured data, where the differences may arise due to the fabrication imperfections, defect sites and grain boundaries on graphene. As the carrier concentration decreases, Fermi energy decreases, and more interband transitions are allowed resulting in a broader and damped resonance curve. In addition, the reason of the blue shift is that the real part of the refractive index changes at different electrical dopings.

In summary, we demonstrated resonance broadening and tuning of split ring resonators by utilizing an epitaxial graphene device with transparent top-gate. We obtained a frequency shift and electrical damping by using the graphene layer between the substrate and SRRs owing to the tunable carrier concentration of graphene, which consequently modulated its optical conductivity. Graphene based nanophotonics is an intense research due to a wide range of applications of this phenomenon. As SRRs are already being realized at optical frequencies,[32,33] it is possible to use these SRRs and graphene-based structures for optical applications such as photovoltaics, ultrafast miniature photodetectors, and optical switches.

[1]A. K. Geim and K. S. Novoselov, Nat. Mater. **6**, 183–191 (2007).
[2]K. S. Novoselov, A. K. Geim, S. V. Morozov, D. Jiang, M. I. Katsnelson, I. V. Grigorieva, S. V. Dubonos, and A. A. Firsov, Nature **438**, 197–200 (2005).
[3]F. H. L. Koppens, D. E. Chang, and F. J. G. de Abajo, Nano Lett. **11**, 3370–3377 (2011).
[4]K. I. Bolotin, K. J. Sikes, Z. Jiang, M. Klima, G. Fudenberg, J. Hone, P. Kim, and H. L. Stormer, Solid State Commun. **146**, 351–355 (2008).
[5]K. S. Novoselov, A. K. Geim, S. V. Morozov, D. Jiang, Y. Zhang, S. V. Dubonos, I. V. Grigorieva, and A. A. Firsov, Science **306**(5696), 666–669 (2004).
[6]Y. Zhang, Y. W. Tan, H. L. Stormer, and P. Kim, Nature **438**, 201–204 (2005).
[7]X. Du, I. Skachko, A. Barker, and E. Y. Andrei, Nat. Nanotechnol. **3**, 491–495 (2008).
[8]Z. Q. Li, E. A. Henriksen, Z. Jiang, Z. Hao, M. C. Martin, P. Kim, H. L. Stormer, and D. N. Basov, Nature Phys. **4**, 532–535 (2008).
[9]F. Wang, Y. Zhang, C. Tian, C. Girit, A. Zettl, M. Crommie, and Y. R. Shen, Science **320**, 206–209 (2008).
[10]F. Bonaccorso, Z. Sun, T. Hasan, and A. C. Ferrari, Nat. Photonics **4**, 611–622 (2010).
[11]T. Hasan, Z. Sun, F. Wang, F. Bonaccorso, P. H. Tan, A. G. Rozhin, and A. C. Ferrari, Adv. Mater. **21**, 3874–3899 (2009).
[12]Z. Sun, T. Hasan, F. Torrisi, D. Popa, G. Privitera, F. Wang, F. Bonaccorso, D. M. Basko, and A. C. Ferrari, ACS Nano **4**, 803–810 (2010).
[13]R. J. Stoehr, R. Kolesov, J. Pflaum, and J. Wrachtrup, Phys. Rev. B **82**, 121408(R) (2010).
[14]T. Gokus, R. R. Nair, A. Bonetti, M. Bhmler, A. Lombardo, K. S. Novoselov, A. K. Geim, A. C. Ferrari, A. A. Green, M. C. Hersam, and A. Hartschuh, in E–MRS Spring Meeting, 2010.
[15]T. Kampfrath, L. Perfetti, F. Schapper, C. Frischkorn, and M. Wolf, Phys. Rev. Lett. **95**, 187403 (2005).
[16]K. F. Mak, J. Shan, and T. F. Heinz, Phys. Rev. Lett. **104**, 176404 (2010).
[17]M. Breusing, C. Ropers, and T. Elsaesser, Phys. Rev. Lett. **102**, 086809 (2009).
[18]X. S. Li, W. W. Cai, J. H. An, S. Kim, J. Nah, D. X. Yang, R. D. Piner, A. Velamakanni, I. Jung, E. Tutuc, S. K. Banerjee, L. Colombo, and R. S. Ruoff, Science **324**, 1312–1314 (2009).
[19]V. V. Khardikov, E. O. Iarko, and S. L. Prosvirnin, J. Opt. **12**, 045102 (2010).
[20]A. Bostwick, T. Ohta, T. Seyller, K. Horn, and E. Rotenberg, Nat. Phys. **3**, 36–40 (2007).
[21]A. Bostwick, F. Speck, T. Seyller, K. Horn, M. Polini, R. Asgari, A. H. MacDonald, and E. Rotenberg, Science **328**, 999–1002 (2010).
[22]J. Kim, H. Son, D. J. Cho, B. Geng, W. Regan, S. Shi, K. Kim, A. Zettl, Y. Shen, and F. Wang, Nano Lett. **12**, 5598–5602 (2012).
[23]Y. Yao, M. A. Kats, P. Genevet, N. Yu, Y. Song, J. Kong, and F. Capasso, Nano Lett. **13**, 1257–1264 (2013).
[24]N. K. Emani, T. F. Chung, X. Ni, A. V. Kildishev, Y. P. Chen, and A. Boltasseva, Nano Lett. **12**, 5202–5206 (2012).
[25]L. A. Falkovsky and A. A. Varlamov, Eur. Phys. J. B **56**, 281–284 (2007).
[26]L. A. Falkovsky and S. S. Pershoguba, Phys. Rev. B **76**, 153410 (2007).
[27]Y. Liu, R. F. Willis, K. V. Emtsev, and T. Seyller, Phys. Rev. B **78**, 201403 (2008).
[28]C. Tegenkamp, H. Pfnur, T. Langer, J. Baringhaus, and H. W. Schumacher, J. Phys.: Condens. Matter **23**, 012001 (2011).
[29]V. W. Brar, S. Wickenburg, M. Panlasigui, C. Park, T. O. Wehling, Y. Zhang, R. Decker, C. Girit, A. V. Balatsky, S. G. Louie, A. Zettl, and M. F. Crommie, Phys. Rev. Lett. **104**, 036805 (2010).
[30]M. M. Ugeda, I. Brihuega, F. Guinea, and J. M. Gomez-Rodriguez, Phys. Rev. Lett. **104**, 096804 (2010).
[31]K. Kim, H. Kang, C. Y. Lee, and W. S. Yun, J. Vac. Sci. Technol. B **31**, 030602 (2013).
[32]K. Aydin, A. O. Cakmak, L. Sahin, Z. Li, F. Bilotti, L. Vegni, and E. Ozbay, Phys. Rev. Lett. **102**, 013904 (2009).
[33]L. Sahin, K. Aydin, G. Turhan-Sayan, and E. Ozbay, J. Nanophotonics **5**, 051812 (2011).